Magnetism of uranium/iron multilayers: I. Fabrication and characterization

2004 J. Phys.: Condens. Matter 16 8491

(http://iopscience.iop.org/0953-8984/16/47/004)

INSTITUTE OF PHYSICS PUBLISHING JOURNAL OF PHYSICS: CONDENSED MATTER

J. Phys.: Condens. Matter **16** (2004) 8491–8505 PII: S0953-8984(04)84361-3

Magnetism of uranium/iron multilayers: I. Fabrication and characterization

A M Beesley[1,7], M F Thomas[1], A D F Herring[1], R C C Ward[2], M R Wells[2], S Langridge[3], S D Brown[1,4], S W Zochowski[5], L Bouchenoire[1,4], W G Stirling[1,4] and G H Lander[6]

[1] Department of Physics, University of Liverpool, Liverpool L69 7ZE, UK
[2] Clarendon Laboratory, University of Oxford, Oxford OX1 3PU, UK
[3] ISIS, Rutherford Appleton Laboratory, Chilton, Oxfordshire OX11 0QX, UK
[4] European Synchrotron Radiation Facility, BP220, F-38043 Grenoble Cedex 09, France
[5] Department of Physics and Astronomy, University College London, London WC1E 6BT, UK
[6] European Commission, JRC, Institute for Transuranium Elements, Postfach 2340, Karlsruhe, D-76125, Germany

E-mail: amb@cmp.liv.ac.uk

Received 3 August 2004, in final form 13 October 2004
Published 12 November 2004
Online at stacks.iop.org/JPhysCM/16/8491
doi:10.1088/0953-8984/16/47/004

Abstract

U/Fe multilayers constitute a magnetic system in which the 3d magnetism of the Fe layers will be modified by hybridization with the U 5f electrons. This paper describes a programme of measurements of the magnetic behaviour of these systems beginning with the fabrication and thorough characterization of the samples. Metallic U/Fe multilayers were prepared by DC sputtering in a UHV chamber. A range of samples with measured U thicknesses, t_U, in the range 18–66 Å and Fe thicknesses, t_{Fe}, from 7 to 108 Å was fabricated. X-ray and neutron reflectivity measurements showed strong peaks indicating good layer structure and gave a determination of the bilayer thickness. X-ray diffraction analysis showed crystalline α-U and α-Fe for layer thicknesses greater than about 20 Å. The α-Fe is strongly textured with (110) planes in the layer plane. The Fe lattice parameter is larger for the case of thin layers, but approaches the bulk value of 2.866 Å at $t_{Fe} \sim 75$ Å. Mössbauer spectra of α-Fe were obtained for $t_{Fe} \geqslant 18$ Å; a non-magnetic component of thickness $\sim$12 Å per layer is always present. The results from these different experimental techniques are combined to present a detailed description of these multilayer systems.

[7] Author to whom any correspondence should be addressed.

1. Introduction

Magnetic multilayers have generated an enormous amount of interest, both in terms of the new fundamental phenomena that can be studied (such as giant magnetoresistance [1], oscillatory interlayer coupling [2], spin-transfer torques [3]), as well as their tremendous technological importance in magnetic recording [4], magnetic random access memory [5], and spintronics. To date, much of this work has focused on 3d and 4f systems. Many different combinations of metals have been studied and used as component magnetic and spacer layers in attempts to attain extreme values of quantities such as magnetic anisotropy for use in magnetic devices. One set of elemental materials that has been only cursorily investigated is that using actinides (elements such as uranium, having an incomplete shell of 5f electrons) as one of the layers. The juxtaposition of actinide layers with layers of strongly magnetic transition metals forms a system whose behaviour will be determined by the interaction of the 5f and 3d electrons.

Early experiments on uranium-based films were performed at the IBM, Yorktown Heights Laboratory in the early 1990s. These showed a number of interesting effects:

(1) Thin film amorphous uranium compounds had completely different properties to their crystalline homologues [6].
(2) Large magnetoresistance effects could be found [7].
(3) Giant magneto-optic rotation could be found in thin films of uranium compounds [8].
(4) When a multilayer composed of amorphous UAs (a ferromagnet at low temperature) and Co was made, the uranium had an induced moment even at room temperature [9].

Efforts to find direct evidence for the moment associated with the U atoms in these amorphous layers in the multilayers using polarized neutrons [10] did not succeed. The effects are certainly small, and the multilayers were deposited on (ferromagnetic) cobalt, which dominates the neutron reflectivity. Later [11], x-ray magnetic circular dichroism was able to confirm the magneto-optic measurements and showed that the U 5f moments were indeed polarized, at room temperature in certain compositions, by their proximity to the Co atoms.

A similar system of this type, the Ce/Fe multilayers, where the interaction occurs between 4f and 3d electron states has also been extensively investigated [12]. A clear magnetic moment is found associated with the Ce atoms. The more recent work of this group, using both resonant x-ray reflectivity and x-ray dichroism techniques [13] has shown that the profile of polarization across the Ce layer may be obtained. In addition, in some samples strong interfacial magnetic anisotropy acts to align the Fe moments normal to the layer plane [14].

In the case of the actinide/transition metal U/Fe, a more extreme behaviour was anticipated as the large orbital moment associated with uranium, and its coupling to the lattice, gives rise to some of the largest known values of magnetic anisotropy in 5f materials [15, 16]. The combination of the uranium orbital moment and the (possible) hybridization of the 5f electrons with those of the Fe 3d shell promised to give rise to a strongly hybridized system, in which the spin direction and rigidity might be engineered. An initial study using resonant magnetic x-ray reflectivity and concentrating on one sample has shown that the uranium is indeed ferromagnetically coupled to the iron for temperatures from 10 to 300 K [17]. Some key questions remain which require a systematic study of U/Fe multilayers with varying uranium and iron thicknesses. These include whether good quality multilayers can be fabricated and characterized in detail, whether the thin film geometry affects the magnetism of the constituent layers, whether the layers interact, and whether the induced uranium moment is affected by the uranium/iron thicknesses.

This paper (I), attempts to answer the first of these questions and in doing so lays a foundation for the subsequent specialized magnetic studies (paper II and following). Here a multi-technique approach utilizing x-ray and neutron reflectivity, x-ray diffraction, and Mössbauer spectroscopy is employed to determine sample quality, layer thicknesses, crystallinity of materials, extent of interfaces, and any inhomogeneities that may occur at the boundaries of the multilayer samples.

2. Fabrication

The U/Fe multilayers were grown at Oxford using a dedicated (single-chamber) UHV, DC magnetron sputtering system. Prior to deposition the chamber was baked, enabling a base pressure of $\approx 10^{-10}$ mbar to be obtained; deposition occurred in a pressure of 5×10^{-3} mbar of purified argon. Because the guns did not have individual shutters and were active throughout the growth run, multilayers were grown by the positioning of the substrate relative to the appropriate gun. The rate of deposition from each gun was obtained by the deposition of single thin layers of each element and the *ex situ* determination of the thickness from a measurement of the Kiessig fringe interval in x-ray reflectivity spectra. Deposition rates of $\sim$2–3 Å s^{-1} were used for the multilayer growth.

In a typical growth run two substrates were loaded into the chamber on a carriage that could be rotated to position either substrate below a selected gun. In this way 'pairs' of samples were grown simultaneously with U and Fe thicknesses of the two samples being related by the ratio of the sputtering rates of the individual guns. The time to reposition the substrates was small compared with the growth time of any individual layer; this was achieved using a UHV feedthrough combined with a precision-engineered head that was computer controlled. Appropriate shielding was used to prevent cross-talk between guns.

In all samples a U layer was deposited first onto the substrate, followed by alternate layers of Fe and U, terminating with an Fe layer. This required that at the start of a growth run one sample received its first U layer before the Fe gun was activated and the same sample obtained its final Fe layer after the U source was switched off. Multilayer samples fabricated in this way are represented as [U(x Å)/Fe(y Å)]n where x and y are layer thicknesses in Å and n is the number of repeats. Glass and sapphire substrates of typical dimensions 12 mm $\times$ 10 mm $\times$ 1 mm thick were used with additional Kapton substrates for transmission Mössbauer spectroscopy (TMS) studies (see below).

A set of 20 samples with different layer thicknesses and U/Fe thickness ratios were fabricated. The measured thicknesses of the U layers were in the range 18–66 Å and those of the Fe layers were in the range 7–108 Å as determined by x-ray and neutron reflectivity measurements described below.

In order to study multilayer samples by TMS it is necessary to use substrates that are transparent to the 14.4 keV Fe^{57} gamma rays. For these studies multilayers were grown on polyimide (Kapton) substrates. In this case the substrate is not sufficiently flat for performing x-ray reflectivity (XRR) measurements but in all cases the Kapton substrate was paired with a glass substrate in the growth process so that the layer thicknesses and quality of these Kapton-based samples could be inferred from measurements on their glass substrate twin. In all studies where results from glass-and Kapton-based samples could be compared, i.e. conversion electron Mössbauer (CEMS) and x-ray diffraction (XRD), no differences were found between them. In the results shown in section 3, samples with reference numbers 2.5, 2.8, 2.9, 2.11, 3.2, 3.4, 3.6, and 3.8 were deposited on a glass substrate and the sample with reference number 3.5 on a Kapton substrate.

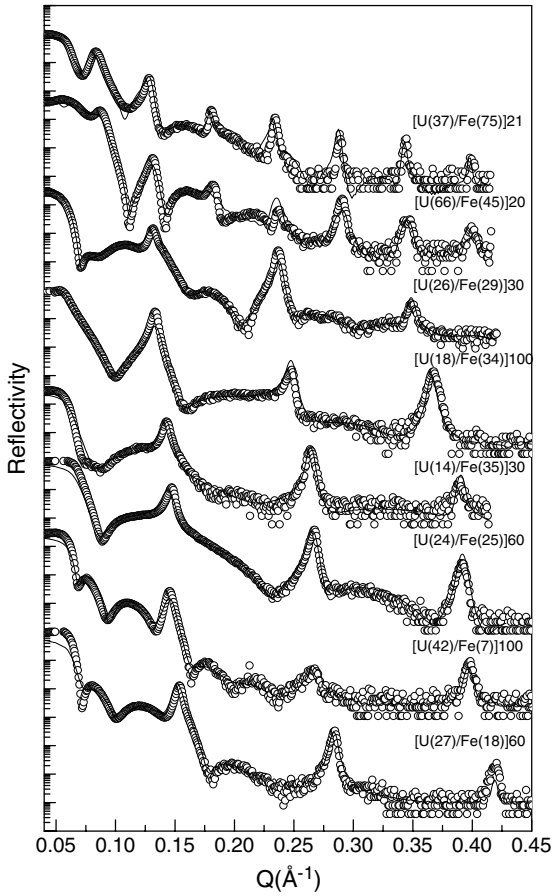

Figure 1. Reflectivity scans taken with x-ray energy of wavelength 1.54 Å (Cu Kα) at room temperature. The open circles are the XRR data and the lines are the result from the fitting program. The scans are presented in order of decreasing sample bilayer thickness from top to bottom.

3. Characterization

3.1. Layer thickness determination

3.1.1. X-ray reflectivity. X-ray reflectivity (XRR) scans were used in order to determine bilayer thicknesses, individual layer thicknesses, and the quality of the layer interfaces for U/Fe multilayer samples grown on glass substrates. The XRR measurements were taken using a Philips X'Pert PRO diffractometer in the Oliver Lodge Laboratory at the University of Liverpool. The sample is mounted on a high resolution goniometer which allows the automatic positioning of the sample in conventional three-circle geometry plus x, y, and z motions. The x-ray source is a 3 kW copper anode tube followed by a focusing mirror and a Ge(220) monochromator, which produces Cu Kα x-rays with a wavelength of 1.540 56 Å. The sealed proportional detector gave 84% efficiency of detection for x-rays of this wavelength.

The reflectivity data were taken as a scan of θ and 2θ from $2\theta = 0°$ to 6°, with step size 0.005° and a counting time of 100 s per point giving a total of ∼16 h per reflectivity curve. Examples of reflectivity spectra are shown in figure 1 in which the normalized intensity of the reflectivity signal is plotted against the momentum transfer normal to the surface defined by

Table 1. Characteristics of multilayer structure obtained by fitting the x-ray and neutron reflectivity scans shown in figures 1 and 2 respectively. The first two columns identify the samples and list the number of bilayer repeats, n. The next two columns list iron and uranium layer thicknesses t_{Fe}, t_U derived from XRR data. The final two columns list similar data obtained from NR scans.

		XRR		NR	
Sample	n	t_{Fe} ±2 (Å)	t_U ±2 (Å)	t_{Fe} ±2 (Å)	t_U ±2 (Å)
2.8	21	75	37	76	38
2.5	20	45	66	46	65
2.9	30	29	26	29	26
3.6	100	34	18	34	18
2.11	30	35	14	35	14
3.8	60	25	24	27	23
3.4	100	7	42	9	40
3.2	60	18	27	19	28

$Q = 2k \sin\theta$, where k is the x-ray wavevector and 2θ is the scattering angle. The open circles correspond to the XRR data and the lines are the best fit to the data. In the figure there is a progressive decrease in U + Fe bilayer spacing from top to bottom of the figure. The large number of peaks generated by the layers confirms the good quality of the multilayers.

The reflectivity scans were fitted using the SPEEDO reflectivity code [18]. The program calculates the reflectivity of x-rays from multilayers with interface regions following the approximation of Névot and Croce [19, 20]. The input model consists of layer thicknesses, optical parameters δ and β (defining the refractive index), and the thickness of the interfaces, for all layers. The thickness of the substrate is modelled as infinite. This program uses simulated annealing and a choice of methods such as dynamical Monte Carlo and acceptance-ratio [21] methods to fit to the data.

The basic model consists of a low density bilayer of Fe/U metal on the top of the glass substrate, followed by a stack of U/Fe bilayers and finally two bilayers of low density iron and uranium oxides. The values of $\delta_{Fe,U}$ and $\beta_{Fe,U}$ were allowed to vary by up to 20% from the U and Fe bulk values. Variable parameters represented the layer and interface thicknesses and optical parameters δ and β of the low density bilayer next to the substrate, the repeated U/Fe layers of the stack, and the two low density oxide bilayers.

Values of the layer thickness are listed in table 1 for a series of multilayers with thicknesses in the range 7 Å $< t_{Fe} <$ 75 Å and 18 Å $< t_U <$ 66 Å. The large Q range accessible coupled with the low structural roughness allow us to determine the equivalent bilayer spacing to an accuracy of ±1 Å. The determinations of individual layer thicknesses depend on less well defined features of the fitting and hence have greater uncertainty (±2 Å). The fits also give an interface region r_i representing roughness and interdiffusion. Consistent values for this parameter were difficult to determine from the fitting procedure but the values were covered by the range $r_i = 8 \pm 5$ Å. It is to be noted that in these fits it is not possible to distinguish between roughness and interdiffusion with the method used.

In this multi-parameter analysis, fitting minima can occur for different sets of parameters. An example of this occurred for sample 2.9 where alternative values of $t_{Fe} = 25$ Å and $t_U = 31$ Å were found to give an equally good fit to the data as with the values quoted. The two sets of values have the same bilayer value but differ in individual thicknesses. The values listed in the table are favoured because they present better agreement with systematics of the growth rates.

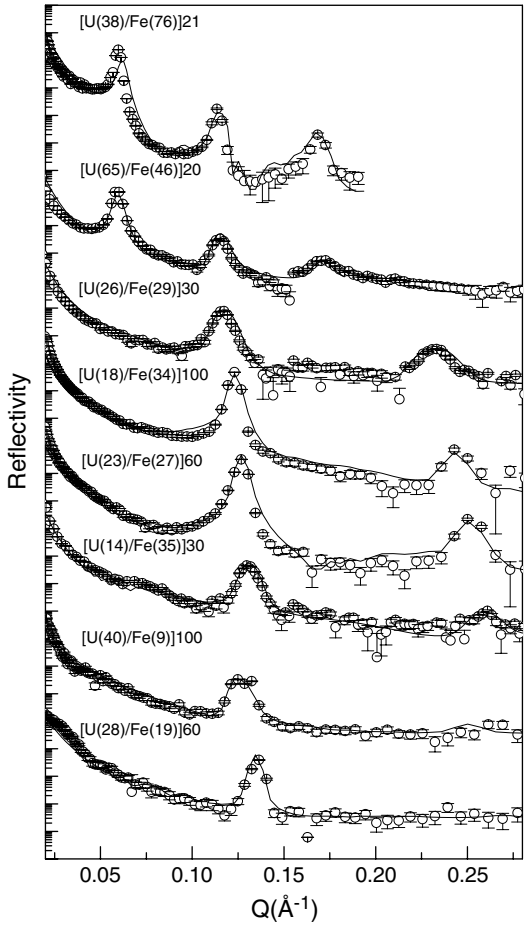

Figure 2. Neutron reflectivity scans taken at room temperature. The circles are the NR data and the lines are the result from the fitting program. These scans are presented in order of decreasing sample bilayer thickness.

3.1.2. Neutron reflectivity. Neutron reflectivity (NR) measurements were performed on the D17 instrument at ILL (Grenoble) and on the CRISP reflectometer at ISIS. Measurements on samples 2.5, 2.9, and 2.11 were made at ILL using a monochromatic neutron beam with a wavelength of 5.3 Å. Measurements on samples 3.2, 3.4, 3.6, and 3.8 were made at CRISP [22] using the time of flight technique. Neutron reflectivity scans of reflected intensity versus Q are shown in figure 2 for the same samples and in the same order as in figure 1. The same change is seen from the top to the bottom scans where the interval ΔQ between layer peaks increases corresponding to decreasing bilayer thickness.

The neutron reflectivity scans were analysed with a program based on the theory of Blundell and Bland [23] and written by Langridge [24]. The input data contain the layer thickness, interface region, nuclear scattering length b, and nuclear number density N for the layer materials. A similar model to that for x-ray reflectivity was used with a bilayer of reduced density adjacent to the substrate, a stack of metallic U and Fe layers, and two bilayers of oxide on the top. In the U/Fe stack the values of b were taken from tables [25] and values of N were varied by up to 20% from the U and Fe bulk values. In the reduced density layers N was

varied to give the best fit. Values taken from x-ray reflectivity proved good starting points for the neutron fits in all cases.

In figure 2 the open circles correspond to the data and the lines are from the best fit model. The good fits give confidence that the model of a reduced density U/Fe bilayer in contact with the glass substrate followed by an extensive stack of metallic U and Fe layers and finally two bilayers of oxidized material is a realistic description of the multilayer. The fitted values for layer thicknesses are listed in table 1. It is seen that these values are in excellent agreement with the values of bilayer thickness and individual layer thickness determined by means of XRR. Values of interface thickness are again difficult to determine consistently from the fits but are covered by the same range $r_i = 8 \pm 5$ Å as found by means of XRR.

The agreement of the values of layer thickness and interface thickness between the reflectivity measurements using completely different probes gives confidence that these features of the samples have been accurately and reliably determined.

3.2. Layer composition

3.2.1. X-ray diffraction. The composition of the sample layers in terms of their crystalline phases, texture, and crystallite size were studied by x-ray diffraction analysis. A number of samples were investigated on the diffraction beamline 2.3 of the SRS at the Daresbury Laboratory. A wavelength, $\lambda = 1.300$ Å (energy $E = 9.535$ keV) was used. For the first studies the sample was fixed at an angle $\omega = 6°$ to the incident beam and the 2θ scan detected diffracted beams from all crystalline planes. The angle $\omega = 6°$ was chosen so that the 1.5 mm height of the beam covered the 12 mm long sample and gave maximum count rate.

The upper trace in figure 3(a) shows the raw data scan for sample 2.5—a sample deposited on a glass substrate. Background scans were made of the substrate and the lower trace of figure 3(a) shows the scan for sample 2.5 with the substrate background subtracted. A fit to the section $2\theta = 20°$–$40°$ of this scan, which contains the main diffraction features, is shown in figure 3(b). In this fit the tabulated d-spacings for α-Fe (bcc), for orthorhombic α-U, and for cubic α-UO_2 were used to calculate the diffraction peak positions; these were kept fixed at the calculated positions. The height and width of the four peaks from α-U were allowed to vary keeping the relative intensities near to the tabulated values. The fit shows the Fe(110) peak at ∼36° and a large feature centred around 30°, which is well described by the overlapping α-U lines. These lines comprise (110) at 29.34°, (021) at 29.84°, (002) at 30.42°, and (111) at 33.42° [26]. The good fit establishes that U is present in the α-phase. The small peak at 23.76° arises from (111) planes of cubic UO_2. No other strong peaks from this oxide are expected in this range of the scan. No peaks from any other phase are seen, either in this section or in the total scan.

A similar $\omega = 6°$ scan for sample 2.8, with substrate background subtracted, is shown in figure 4(a). The same features are seen in this scan as in the range 20°–40° of figure 3(b). In the range $2\theta > 40°$ overlapping α-U peaks at 50°(131) and 53°(023) give rise to the feature at about 52° and the Fe(211) peak is seen at ∼67°. This spectrum is contrasted with the lower scan, in which the sample and two-theta circles move in a coupled θ–2θ motion maintaining the x-ray photon momentum change in the direction normal to the sample surface. In figure 4(b) the scan picks out crystal planes lying in the plane of the sample (layers) and the large enhancement of diffraction intensity from the Fe(110) planes indicates that the iron is highly textured with the (110) planes lying in the plane of the multilayer. This is confirmed by the absence of the (211) peak in the θ–2θ scan showing that these planes are not in the layer plane. The small peak at $2\theta \sim 79°$ arises from Fe(220). Similar strong texturing of the U layers is not observed in the θ–2θ scan; any texturing within the U layers must be small.

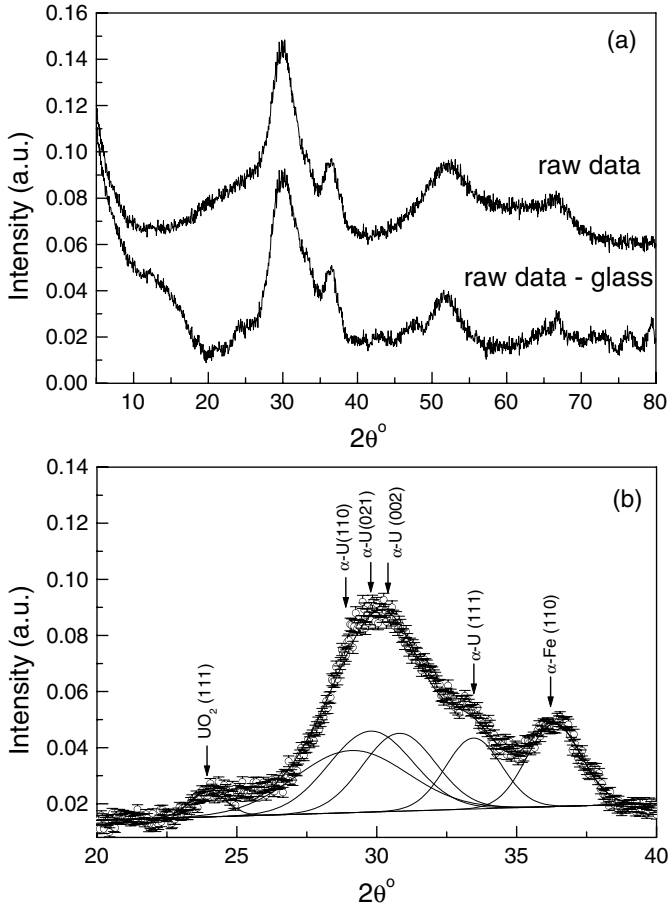

Figure 3. (a) X-ray diffraction data from sample 2.5 ([U(66)/Fe(45)]20) showing raw data and the spectrum after subtraction of the glass substrate background. (b) Analysis of the section of the background subtracted spectrum. The profile shows peaks characteristic of α-Fe, α-U, and UO_2.

Similar scans were recorded for other samples where peaks with larger linewidths were observed for samples with thinner layer thicknesses. No diffraction peaks were observed for Fe layers of thickness <18 Å. Such a limit is more difficult to establish for the overlapping peaks of U but no definitive uranium peaks were observed for U layer thicknesses of <20 Å. Scans of samples on Kapton substrates showed similar features to those for samples deposited on glass substrates. Detailed comparison of crystalline quality between the two sets of samples is hampered by the fact that for Kapton-based samples the layer thickness cannot be determined directly by reflectivity measurements. However, taking thicknesses of the Kapton samples from those made as a pair with a glass-based sample (see section 2 above), the quality of samples on Kapton substrates appeared to be similar to that of ones on glass.

By monitoring the position of the Fe(110) peak the lattice parameter of the Fe layers could be determined and is shown in figure 5(a) as a function of the Fe layer thickness. These fits were performed on the θ–2θ scans giving the lattice constant in the direction normal to the layer plane. However, in each case the peak position from the fixed ω–2θ scan agreed with that of the θ–2θ scan, indicating the same lattice constant in the plane. For the thickest Fe

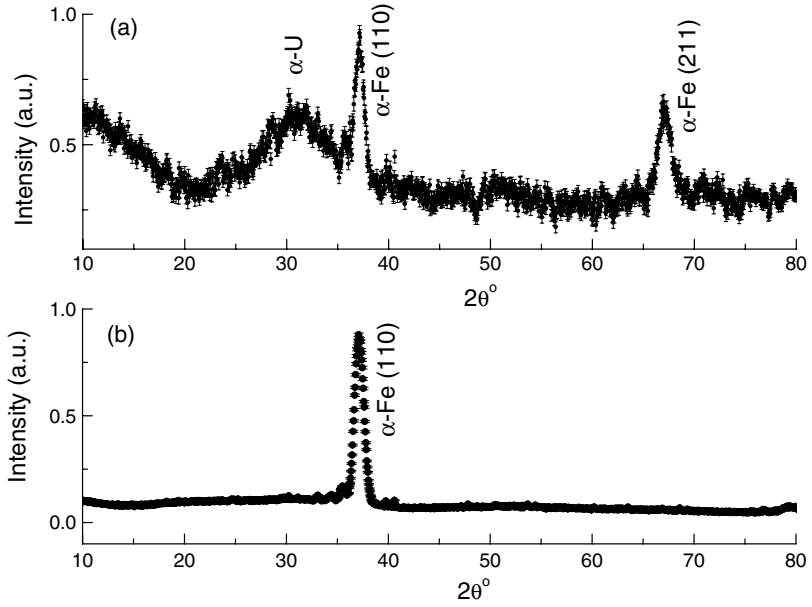

Figure 4. Comparison of x-ray diffraction spectra of sample 2.8 ([U(37)/Fe(75)]21) taken with (a) a fixed sample–2θ scan and (b) with a θ–2θ scan. The enhancement of the Fe(110) peak and disappearance of the Fe(211) peak in the lower spectrum indicate a high degree of texture in the Fe layers with the (110) planes parallel to the layer surfaces.

layer (75 Å) the value of **a** approaches the room temperature bulk value of $\mathbf{a} = 2.866$ Å but for smaller values of the Fe layer thickness the lattice constant shows a significant increase.

Using the Scherrer equation [27] and the fitted linewidth for the Fe(110) peak in the fixed ω–2θ scans, it was possible to calculate the in-plane particle size of the crystalline iron in these multilayers. The results are plotted in figure 5(b). It can be observed that the crystalline particle size for Fe in each multilayer is less than or equal to the thickness of Fe determined by reflectivity measurements.

3.2.2. Mössbauer spectroscopy. The segment of the samples seen by Mössbauer spectroscopy is the iron layer including both interface regions. Figure 6 shows conversion electron Mössbauer spectra (CEMS) of six representative samples taken at room temperature (300 K). The samples are identified and the fitting parameters listed in table 2, where the samples are ranked by decreasing iron thickness, the uppermost spectrum being of a sample with an Fe layer thickness of 75 Å whereas the lowest spectrum is that of a sample having an Fe layer thickness of 18 Å.

The spectra are fitted with up to three basic spectrum components whose relative areas change with Fe layer thickness as listed in table 2. These basic components are:

(1) A sextet with narrow lines and a hyperfine field, $B_{\mathrm{hf}} \sim 32.8$ T, which is characteristic of crystalline bcc iron.
(2) A sextet with broader lines and a smaller hyperfine field, $B_{\mathrm{hf}} \sim 30.0$ T.
(3) A doublet component corresponding to iron that is not magnetically ordered at 300 K.

In both sextet components the hyperfine field is seen to decrease slightly as the Fe layer thickness decreases, presumably reflecting the lower ordering temperature of samples with thinner Fe layers.

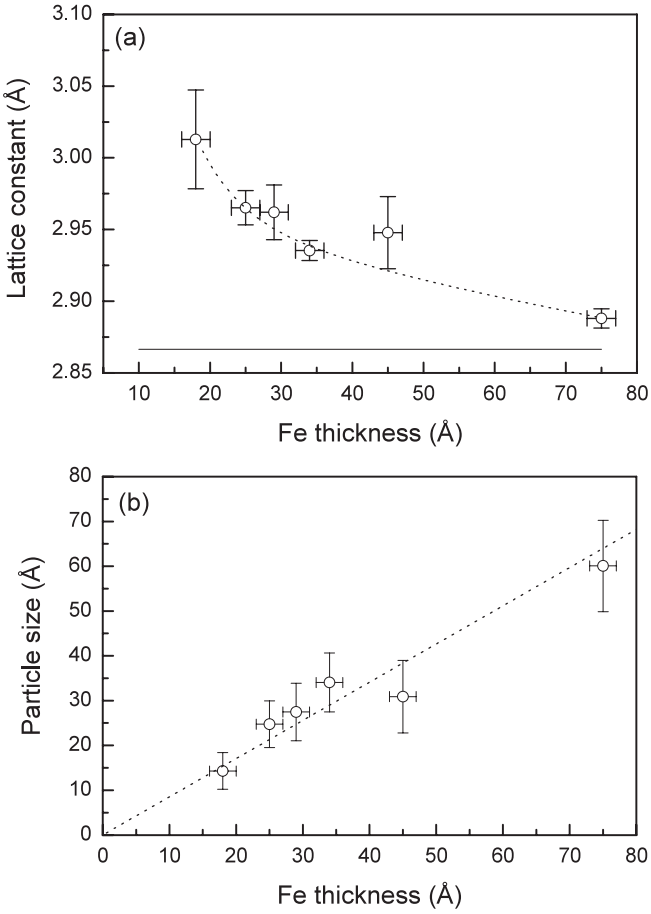

Figure 5. The iron lattice constant **a** (a) and particle size (b) as a function of the Fe thickness in the multilayers, deduced from the position and width of the Fe(110) peak in x-ray diffraction scans. The solid line in (a) corresponds to the bulk iron lattice constant 2.866 Å. The effect of the Fe thickness on the lattice constant and particle size is shown by dashed lines which are a guide to the eye.

The relative areas of each basic spectrum component, listed in table 2, reflect the proportion of iron atoms in each environment. Thus for the 75 Å Fe layer sample most of the iron is present as crystalline bcc Fe whereas for the 18 Å Fe layer sample the majority of the Fe is not magnetically ordered. Values of the proportion R of non-magnetic iron are listed in table 2 and the product of R and the iron layer thickness t_{Fe}, gives t_{i}—the thickness of non-magnetic iron per layer segment. It is seen that t_{i} is essentially constant at $t_{\mathrm{i}} = 12(2)$ Å across the whole range of samples. This suggests that the non-magnetic iron occurs at the interfaces and the magnetic iron is in the remainder of the layers. Whereas it is not essential that the thickness of the non-magnetic interface iron should be exactly equal to the summed interface region seen in the x-ray and neutron reflectivity measurements, the closeness of these independent measures of the interface region reinforces the picture of the layer structure with interfaces of ∼6–8 Å thickness.

The interpretation of the Fe environments giving rise to the three basic components seen in the Mössbauer spectra is:

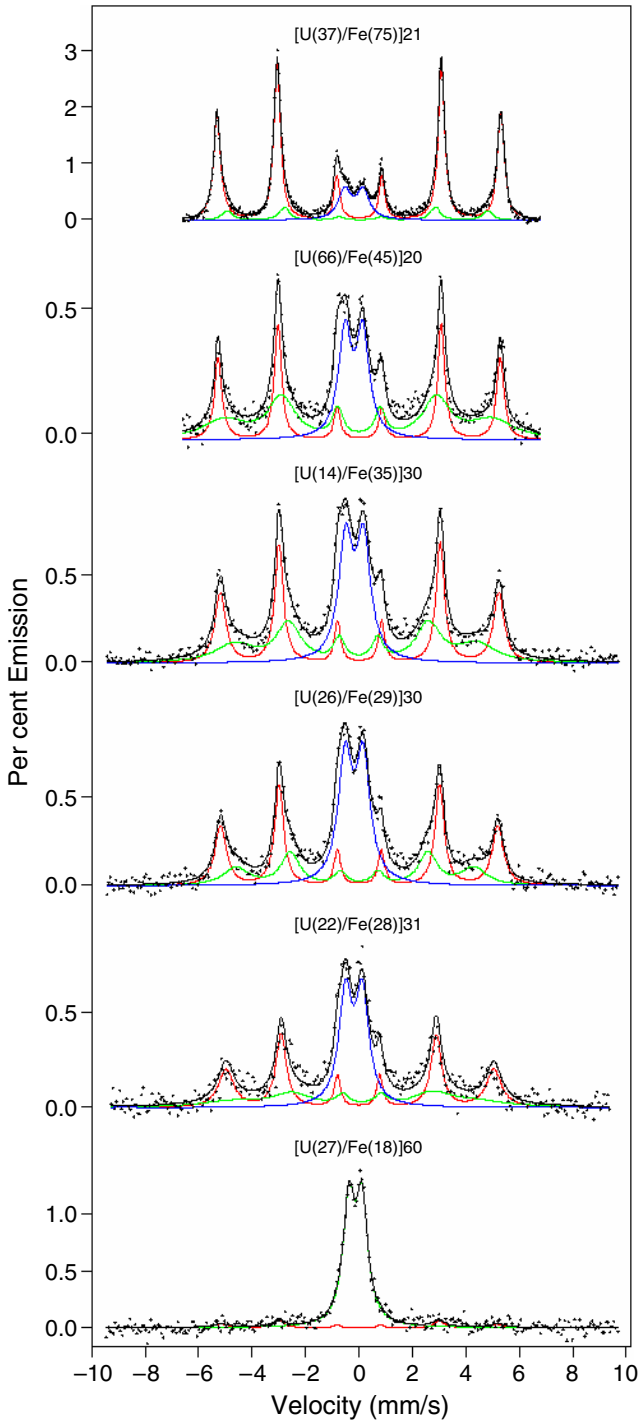

Figure 6. Conversion electron Mössbauer spectra (CEMS), taken at 300 K. The change in the relative areas of the sextet and the doublet components as the Fe layer thickness decreases indicates the presence of non-magnetic iron at the interfaces of the iron layers. The Mössbauer parameters resulting from the fits are listed in table 2.

(This figure is in colour only in the electronic version)

Table 2. Mössbauer parameters from fits to the CEMS spectra shown in figure 6. Layer thicknesses are as defined in table 1. The parameters of the hyperfine field, B_{hf}, and isomer shift, δ, define the profiles of the components. The area A determines their relative abundance. The factor R is the ratio of the non-magnetic component area to the total area, and reflects the proportion of non-magnetic iron residing in the two interfaces of an Fe layer. The final column, headed t_i, lists the effective thickness of the non-magnetic Fe component.

Sample	t_{Fe} (Å)	t_U (Å)	B_{hf} (T) (±0.2)	δ (mm s^{-1}) (±0.01)	A (%) (±5%)	R	t_i (Å) (±2)
2.8	75	37	32.8	0.01	76	0.14	10.5
			30.1	−0.01	10		
			0	−0.20	14		
2.5	45	66	32.7	0.02	31		
			31.0	−0.01	43	0.26	11.7
			0	−0.19	26		
2.11	35	14	32.3	0.02	36		
			28.0	−0.07	34	0.30	10.5
			0	−0.16	30		
2.9	29	26	32.1	0.01	31		
			29.2	0.02	30	0.39	11.3
			0	−0.18	39		
2.12	30	21	31.0	0.02	38		
			28.0	−0.04	26	0.36	10.8
			0	−0.19	36		
3.2	18	27	32.0	0.00	10	0.90	16.2
			0	−0.13	90		

(1) Component 1 arises from crystalline bcc iron in which each Fe atom has eight Fe nearest neighbours and six Fe next nearest neighbours.
(2) Component 2—a sextet with decreased hyperfine field and broadened linewidths—is consistent with a bcc iron structure in which the iron atoms have some non-magnetic ions within the range of their magnetic interactions—for example because of proximity to the interface.
(3) Component 3, the non-magnetic doublet, requires further investigation to establish whether it is caused by the formation of an intermetallic compound (UFe_2) at the interface, whether it is of similar origin to the doublet observed in analogous Ce/Fe multilayers, or, more basically, whether the doublet arises from paramagnetic or diamagnetic Fe atoms.

Information on the first two hypotheses for component 3 is shown in the transmission Mössbauer spectrum (TMS) of figure 7(a). This spectrum is taken at 4.2 K on sample 3.5, [U(42)/Fe(7)]101, Kapton-backed. The spectrum of this sample at 300 K contains the doublet component only and in figure 7(a) it can be seen that the spectrum remains as a doublet and does not show magnetic splitting at 4.2 K. This is not consistent with the intermetallic compound UFe_2, which orders magnetically at 167 K [28, 29] to give a magnetically split spectrum. It is also not consistent with the Ce/Fe multilayer system, in which the room temperature doublet component shows magnetic splitting consistent with impure metallic iron at 4.2 K [30].

Whether this doublet component seen in these U/Fe multilayer systems arises from Fe atoms carrying a magnetic moment (paramagnetic) or zero magnetic moment (diamagnetic) can be investigated via the lower spectrum in figure 7(b). This spectrum, recorded at 4.2 K, is for the same sample as above with a field $B_a = 8$ T applied in the plane of the layers. The total magnetic splitting seen in the Mössbauer spectrum will be $B_a - B_{int}$, where B_{int} is the hyperfine field produced by the (magnetic) atom at the Fe^{57} nucleus. In an atom with no

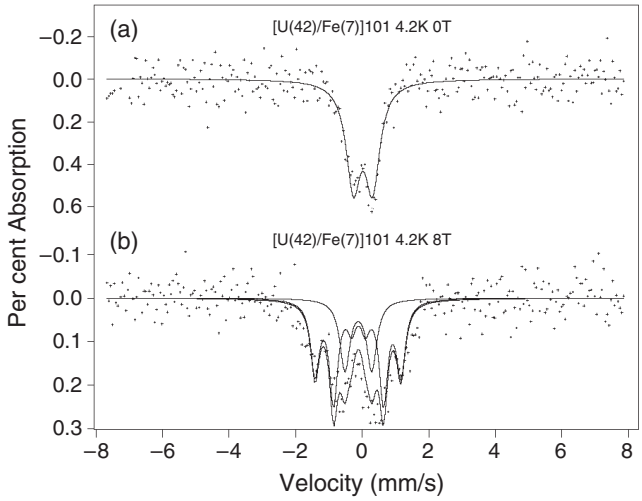

Figure 7. Transmission Mössbauer spectra taken at 4.2 K for sample 3.5 ([U(42)/Fe(7)]101 on a Kapton substrate). (a) The spectrum shows that the non-magnetic iron seen at 300 K in figure 6 does not order at 4.2 K. (b) The spectrum, in an applied field $B = 8.0$ T, shows that the majority of the iron atoms in the sample are in a diamagnetic state.

magnetic moment, $B_{\rm int} = 0$ and the spectrum splitting would be $B_{\rm a} = 8$ T, whereas any $B_{\rm int}$ arising from an Fe atom with a magnetic moment (and now aligned by the applied field) would modify the magnetic splitting seen in the spectrum. Although the spectrum is not of very good quality (the sample is extremely thin for TMS)—it is seen that the majority component is magnetically split with a field of $8(\pm 0.5)$ T consistent with these Fe atoms having no magnetic moment (or alternatively but improbably with $B_{\rm int} = -16$ T).

The magnetic phases grown in the fabrication of these U/Fe multilayers show some similarities to and some differences from Fe/rare-earth (RE) multilayers reported in the literature. In evaporated Fe/Gd multilayers [31] a magnetic phase identified as amorphous iron is detected at interfaces whereas in Ce/Fe [30] and in the present U/Fe multilayers this is not present. As noted above, the doublet component observed at room temperature splits into a magnetic sextet at 4.2 K in Ce/Fe systems but remains unsplit at this temperature in U/Fe.

Further information from the Mössbauer spectra of figure 6 arises from the relative intensities of the lines of the magnetic sextet components. Reading from lower to higher velocity the lines have relative intensities 3:4:1:1:4:3 which indicates that the Fe moments are perpendicular to the gamma ray beam and lie in the plane of the layer within the experimental accuracy. No spectrum components corresponding to iron oxides (which would have hyperfine fields $\sim$50 T) are seen in the wings of the spectra of figure 6. Thus oxidation of the iron layers, seen in the modelling of the upper layers of the reflectivity scans, is insufficient in quantity to be observable by this technique.

4. Summary

The scans and spectra reported in this paper lead to a picture of the samples as a repeated U/Fe layer structure in which the top two bilayers show some oxidation, there follows a uniform stack of metallic layers, and the sample terminates with a reduced density bilayer in contact with the glass substrate. In this structure of n repeats the uniform stack consists of $n - 3$ bilayers—17 bilayers in the thinnest stack (sample 2.5) to 97 bilayers in samples 3.6 and 3.4.

Thus the data shown in the figures above arise overwhelmingly from the stack of metallic layers—the multilayer structure. Subsequent to the fabrication of the multilayers made for this study, we now have a system in which a cap layer can be deposited to prevent oxidation at the top of the multilayer.

The sputtering technique, described in section 2, fabricated well defined layer structures as evidenced by the many layer peaks in the x-ray reflectivity scans of figure 1. The peak positions determine the U + Fe bilayer thickness ($t_U + t_{Fe}$) accurately (± 1 Å) and the values are consistent with those determined from the neutron reflectivity scans of figure 2. Individual layer thicknesses t_U and t_{Fe} are obtained from fits to the detailed peak intensities and profiles between peaks. Fits to the scans involve quite large numbers of variable parameters ($\sim$16 in a normal fit). In these circumstances there can be more than one fitting minimum—thus a good fit may not determine the parameters uniquely. In accepting values of t_U and t_{Fe} for table 1 these values had to provide not only a good fit separately for x-ray and neutron reflectivity scans but also had to match the systematic relation between thickness determined by reflectivity and the nominal thickness set up in the fabrication process. Individual values of t_U and t_{Fe} in table 1 satisfy these requirements and are accurate to $\sim$2 Å. Evidence for oxidation of the top two bilayers and the reduced density bilayer in contact with the substrate comes from the requirement to include these features in detailed fits to scans of all the samples studied.

X-ray diffraction studies show that the metallic layers of the stack are composed of α-Fe and α-U. Comparison of 2θ (powder) scans with θ–2θ scans shows that the Fe layers are highly textured with the (110) planes parallel to the layer plane. Overlapping lines make it difficult to determine whether there is any texture in the U layers. Analysis of the fitted linewidths of the diffraction peaks gives grain sizes of $\sim t_{Fe}$ in the Fe layers. Oxidation of the U layers is confirmed by the detection of a small UO_2 peak for all samples. Detailed fits of the x-ray reflectivity scans, shown in figure 1, indicate that this oxidation of the uranium is predominantly in the top few layers. The lattice parameter for α-Fe is found to approach the bulk value of 2.866 Å for the thickest Fe layers (75 Å), but to be increased by 3% for layers of $\sim$20 Å thickness.

The Mössbauer spectra of figure 6 show that the iron layers consist of α-Fe but also that all samples contain a component of non-magnetic iron occurring at the interfaces. By elimination of other possibilities, the non-magnetic Mössbauer component appears likely to arise from Fe atoms existing in a local environment of poor crystallinity or non-crystallinity at the layer interfaces. The thickness of this non-magnetic component is found to be 12(2) Å per layer (two interfaces), independently of the layer thickness. This value is close to the interface thickness per layer (two interfaces) of 16(10) Å indicated by the x-ray and neutron reflectivity fits. Whereas there is no requirement for these values to be exactly the same, the results suggest that the interface exists as an amorphous (non-magnetic) region of thickness $\sim$6–8 Å.

This investigation is the first in-depth study of U/Fe multilayers. It is been shown that the combination of scattering and spectroscopic techniques, using x-rays, neutrons, and gamma rays as probes, can construct a detailed picture of the structure of U/Fe multilayers. These results constitute a firm foundation of structure on which to base subsequent detailed magnetic studies.

Acknowledgments

A M Beesley is grateful for the support of an ORS award. A D F Herring acknowledges the receipt of an EPSRC research studentship. We gratefully acknowledge the support of Dr P Donovan and the technical support of Mr K Belcher at Oxford. We would like to thank the local contacts at the SRS (s2.3), ILL (D17) and ISIS (CRISP) for their support during the experiments.

References

[1] Tsymbal E Y and Pettifor D G 2001 *Solid State Phys.* **56** 113
[2] Bruno P 1993 *J. Magn. Magn. Mater.* **121** 248
[3] Berger L 2002 *J. Appl. Phys.* **91** 6795
[4] Coehoorn R 1999 *Magnetic Multilayers and Giant Magnetoresistance* (*Springer Series in Surface Sciences* vol 37) (Berlin: Springer) p 65
[5] Tehrani S *et al* 2003 *Proc. IEEE* **91** 703
[6] Frietas P P, Plaskett T S, Moreira J M and Amaral V S 1988 *J. Appl. Phys.* **64** 5453
Plaskett T S, McGuire T R, Fumagalli P, Gambino R J and Bojarczuk N A 1991 *J. Appl. Phys.* **70** 5855
[7] Freitas P P, Plaskett T S and McGuire T R 1988 *J. Appl. Phys.* **63** 3746
Freitas P P and Plaskett T S 1990 *J. Appl. Phys.* **67** 4901
[8] Gambino R J, Plaskett T S, McGuire T R and McElfresh M W 1991 *J. Appl. Phys.* **69** 4750
Fumagalli P, Plaskett T S, McGuire T R, Gambino R J and Bojarczuk N 1992 *Phys. Rev.* B **46** 6187
Fumagalli P, Plaskett T S and McGuire T R 1993 *J. Appl. Phys.* **73** 6112
[9] Fumagalli P, Plaskett T S, Weller D, McGuire T R and Gambino R J 1993 *Phys. Rev. Lett.* **70** 230
[10] Mannix D, Stirling W G, Bucknall D G, Haycock P W, Brown S D, Lander G H and Plaskett T S 1997 *Physica* B **234–236** 470
[11] Kernavanois N, Mannix D, Dalmas de Réotier P, Sanchez J-P, Yaouanc A, Rogalev A, Lander G H and Stirling W G 2004 *Phys. Rev.* B **69** 054405
[12] Arend M, Finazzi M, Schutte O, Münzenberg M, Dias A-M, Baudelet F, Giorgetti Ch, Dartyge E, Schaaf P, Kappler J-P, Krill G and Felsch W 1998 *Phys. Rev.* B **57** 2174 and references therein
[13] Jaouen N, Tonnerre J M, Raoux D, Bontempi E, Ortega L, Münzenberg M, Felsch W, Rogalev A, Dürr H A, Dudzik E, Van der Laan G, Maruyama H and Suzuki M 2002 *Phys. Rev.* B **66** 134420
[14] Case G S, Thomas M F, Lucas C A, Mannix D, Boni P, Tixier S and Langridge S 2001 *J. Phys.: Condens. Matter* **13** 9699–712
[15] Lander G H, Brooks M S S, Lebech B, Brown P J, Vogt O and Mattenberger K 1990 *Appl. Phys. Lett.* **57** 989
[16] Brooks M S S and Johansson B 1993 *Handbook of Magnetic Materials* vol 7, ed K H J Buschow (Amsterdam: North-Holland) pp 139–230
[17] Brown S D, Beesley A, Herring A, Mannix D, Thomas M F, Thompson P, Bouchenoire L, Langridge S, Lander G H, Stirling W G, Ward R C and Zochowski S W 2003 *J. Appl. Phys.* **93** 6519–21
[18] Knewtson M and Suter R M, Department of Physics of the University of Pittsburgh. US http://x2d.phys.cmu.edu/soft.html
[19] Croce P 1977 *J. Opt.* **8** 127–39
[20] Névot L and Croce P 1980 *Rev. Phys. Appl.* **15** 761–79
[21] Bouzida D, Kumar S and Swendsen R 1992 *Phys. Rev.* A **45** 8894
[22] Felici R, Penfold J, Ward R C and Williams W G 1988 *Appl. Phys.* A **45** 169
[23] Blundell S J and Bland J A C 1993 *J. Magn. Magn. Mater.* **121** 185
[24] Langridge S, Rutherford Appleton Laboratory http://www.rl.ac.uk/largescales/
[25] NIST Centre for Neutron Research http://www.ncnr.nist.gov/resources/n-lengths/index.html
[26] MINCRYST, Institute of Experimental Mineralogy, Russian Academy of Sciences http://database.iem.ac.ru/mincryst/
[27] D'Agostino A T 1992 *Anal. Chim. Acta* **262** 269–75
[28] Tsutsui S, Nakada M, Kobayashi Y, Nasu S, Haga Y and Ōnuki Y 2001 *Hyperfine Interact.* **133** 17–21
[29] McGuire T K and Herber R H 1983 *Solid State Commun.* **48** 393–5
[30] Case G S, Thomas M F, Lucas C A, Mannix D, Boni P, Tixier S and Langridge S 2001 *J. Phys.: Condens. Matter* **13** 9699–712
[31] Landes J, Sauer Ch, Kabius B and Zinn W 1991 *Phys. Rev.* B **44** 8342–5